ANNUAL REVIEWS

Annual Review of Condensed Matter Physics

Nonreciprocal Transport and Optical Phenomena in Quantum Materials

Naoto Nagaosa[1] and Youichi Yanase[2]

[1]RIKEN Center for Emergent Matter Science (CEMS), Wako, Japan; email: nagaosa@riken.jp

[2]Department of Physics, Kyoto University, Kyoto, Japan; email: yanase@scphys.kyoto-u.ac.jp

Annu. Rev. Condens. Matter Phys. 2024. 15:63–83

First published as a Review in Advance on October 31, 2023

The *Annual Review of Condensed Matter Physics* is online at conmatphys.annualreviews.org

https://doi.org/10.1146/annurev-conmatphys-032822-033734

Keywords

nonreciprocal responses, magnetochiral anisotropy, geometric Berry phase, superconducting diode, shift current, photovoltaic effect

Abstract

In noncentrosymmetric materials, the responses (for example, electrical and optical) generally depend on the direction of the external stimuli, called nonreciprocal phenomena. In quantum materials, these nonreciprocal responses are governed by the quantum geometric properties and symmetries of the electronic states. In particular, spatial inversion ($\mathcal{P}$) and time-reversal ($\mathcal{T}$) symmetries play crucial roles, which are also relevant to the geometric Berry phase. Here, we give a comprehensive review of the nonreciprocal transport and optical responses including (*a*) the magnetochiral anisotropy, i.e., the nonlinear resistivity with respect to the electric field, in semiconductors and metals, (*b*) the nonreciprocal transport in superconductors such as the nonreciprocal paraconductivity and the superconducting diode effect in bulk and Josephson junctions, and (*c*) the second-order nonlinear optical effects in the electric field of light, including the geometric shift current in nonmagnetic systems, magnetic systems, and superconductors.

1. INTRODUCTION

Correct definition being put aside, nonreciprocity refers to the breakdown of equivalence between the right mover and the left mover. Such phenomena are ubiquitous, and several canonical systems can be found in condensed matter. A typical example is the diode, which has asymmetric current–voltage characteristics between the right and left directions. Diodes are one of the fundamental building blocks of modern technology due to their nonreciprocal properties. Because of their utility and fundamental interest, extensive research has long been conducted on nonreciprocal effects in condensed matter and devices.

Whereas early studies focused primarily on classical mechanisms, recent works have revealed the close relationship between nonreciprocal phenomena and the quantum properties of the materials. In quantum materials, a variety of fascinating concepts have been explored including topology and quantum geometry of wave functions, correlations and dissipation in many-body states, and exotic phase transitions and symmetry breaking due to quantum condensation. These quantum materials provide an intriguing platform for nonreciprocal phenomena (1–3).

In this article, we review recent developments in nonreciprocal phenomena in quantum materials from a theoretical perspective and describe related experiments. In the following, we focus on electric response, i.e., nonreciprocal transport and optical phenomena. Platforms range from metals, insulators, and semiconductors to magnetic materials and superconductors. Unique effects in superconductors are also outlined: nonreciprocal paraconductivity, superconducting diode effects, and superconducting nonreciprocal optics.

2. NONRECIPROCAL TRANSPORT IN SEMICONDUCTORS AND METALS

The time-reversal symmetry operation $\mathcal{T}$ plays an essential role in linear and nonlinear responses. For spin 1/2 particles such as electrons, it is defined by $\mathcal{T} = i\sigma_y\mathcal{K}$, where $\mathcal{K}$ is the complex conjugation and σ_y is the Pauli matrix. The time-reversal symmetry of the Hamiltonian can be expressed as $\mathcal{T}H(\boldsymbol{B})\mathcal{T}^{-1} = H(-\boldsymbol{B})$ with $\boldsymbol{B}$ being the magnetic field representing the $\mathcal{T}$-breaking field. This leads to Onsager's reciprocal theorem given by (4, 5)

$$\kappa_{AB}(\omega, \boldsymbol{B}) = \varepsilon_A\varepsilon_B\kappa_{BA}(\omega, -\boldsymbol{B}), \quad 1.$$

where $\kappa_{AB}(\omega)$ is the response function of the observable A to the field h_B with the perturbation Hamiltonian $H' = -h_B B$, i.e., $< A > (\omega, \boldsymbol{B}) = \kappa_{AB}(\omega)h_B(\omega, \boldsymbol{B})$. Here, $\varepsilon_A = \pm 1$ ($\varepsilon_B = \pm 1$) specifies the even (+1) or odd (−1) nature of A (B) with respect to the time reversal. When the component of the wave vector $\boldsymbol{q}$ is considered, Equation 1 turns into

$$\kappa_{ab}(\boldsymbol{q}, \omega, \boldsymbol{B}) = \varepsilon_a\varepsilon_b\kappa_{ba}(-\boldsymbol{q}, \omega, -\boldsymbol{B}). \quad 2.$$

Transport properties correspond to the limit $\boldsymbol{q} \to \boldsymbol{0}$ first, i.e., $\sigma_{\mu\nu}(\boldsymbol{q} = \boldsymbol{0}, \omega, \boldsymbol{B})$. Rikken gave an interesting heuristic argument regarding $\boldsymbol{q}$ as the momentum of electrons and, hence, the current $\boldsymbol{I}$. Based on this argument, he proposed an empirical formula (6–9) in which the resistivity R is given by

$$R = R_0(1 + \beta\boldsymbol{B}^2 + \gamma_{\mu\nu}\boldsymbol{B}_\mu I_\nu), \quad 3.$$

where R_0 is the linear resistivity at zero magnetic field, I is the current, β is the coefficient of the magnetoresistance, and the last term represents the directional nonlinear resistivity with $\gamma_{\mu\nu}$ determined by the symmetry of the system. This nonlinear nonreciprocal transport in systems with broken inversion symmetry $\mathcal{P}$ is named magnetochiral anisotropy (MCA). (Note that γ' is also used by replacing the current I by current density j in Equation 3, which is sample size

independent and has the unit of $T^{-1}\,A^{-1}\,m^2$.) However, Onsager's theorem is applicable only to the linear response, whereas Equation 3 describes nonlinear response. Therefore, Rikken's argument is not an exact statement.

From the viewpoint of the electronic states in solids, i.e., Bloch wave functions and band structure, $\mathcal{T}$ relates the two states $u_n(\boldsymbol{k},\sigma)$ and $u_n(-\boldsymbol{k},-\sigma)$, where u_n is the periodic part of the Bloch wave function. Therefore, the energy dispersion satisfies $\varepsilon_\sigma(\boldsymbol{k}) = \varepsilon_{-\sigma}(-\boldsymbol{k})$, and this symmetry prohibits nonreciprocal charge transport, whereas the spin transport can be asymmetric in conventional Boltzmann transport theory. With magnetic field $\mathcal{B}$ or magnetization M, the energy dispersion becomes asymmetric between $\boldsymbol{k}$ and $-\boldsymbol{k}$, and nonreciprocal charge resistivity becomes possible. Experimentally, γ is usually of the order of 10^{-3}–$10^{-1}\ T^{-1}\,A^{-1}$, and the nonreciprocal part of the resistivity is very small, less than 1% (6–9), which is in sharp contrast to rectification by pn junctions. This can be understood in terms of an explicit example, i.e., the two-dimensional Rashba model under an external magnetic field:

$$H_{\mathrm{R}} = \frac{\hbar^2 k^2}{2m} + \alpha_{\mathrm{R}}(k_x\sigma_y - k_y\sigma_x) - \boldsymbol{B}_y\sigma_y, \qquad 4.$$

where α_{R} is the Rashba coupling strength corresponding to the polar axis along the z direction and the magnetic field applied along the y direction. One can easily see that the energy eigenvalues are given by

$$\varepsilon_\pm(\boldsymbol{k}) = \frac{\hbar^2 k^2}{2m} \pm \sqrt{(\alpha_{\mathrm{R}}k_x - \boldsymbol{B}_y)^2 + (\alpha_{\mathrm{R}}k_y)^2} \qquad 5.$$

and are asymmetric between k_x and $-k_x$ by the factor $\alpha_{\mathrm{R}}\boldsymbol{B}_y k_x$ in the square root. Therefore, the perturbation that induces the nonreciprocal transport is of the order of $\sqrt{\lambda_{\mathrm{R}}\boldsymbol{B}_y}$, where $\lambda_{\mathrm{R}} = \alpha_{\mathrm{R}}k_{\mathrm{F}}$ (k_{F}: Fermi wave number) is the spin–orbit interaction energy and $\boldsymbol{B}_y$ is the Zeeman energy, which is usually much smaller than the kinetic energy $\varepsilon_{\mathrm{F}} \cong \frac{\hbar^2 k_{\mathrm{F}}^2}{2m}$ in metallic systems. However, when the kinetic energy ε_{F} is small and/or the spin–orbit interaction is large, the nonreciprocal transport can be enhanced. This situation is realized in a polar semiconductor BiTeBr showing a large bulk Rashba splitting (10). The analysis based on the Boltzmann transport theory using Equations 4 and 5 (with the dispersion along the c axis) gives quantitative agreement with the experimental observations. Angle-resolved photoemission spectroscopy provides the parameters for the band structure. Furthermore, the coefficient γ_{yx} is independent of the relaxation time τ and, hence, is an intrinsic quantity of the band structure similar to the Hall coefficient. Therefore, one can predict γ_{yx} without any fitting parameters in this material to leading order in τ. GeTe shows also bulk Rashba splitting, showing MCA at room temperature due to the nonlinear magnetoresistance and the spin texture in momentum space (11). A review article for nonreciprocal effects in (quasi-)two-dimensional van der Waals nanostructures is found in Reference 3.

There are several ways to enhance MCA. One is to design materials and their band structures. A Weyl fermion system with broken $\mathcal{P}$ symmetry has been proposed (12). In this system, the chiral anomaly induces a charge imbalance Q_5 between the Weyl node and anti-Weyl node expressed by $Q_5 \simeq \tau\boldsymbol{E}\cdot\boldsymbol{B}$, where τ is the relaxation time. This results in a change in the conductivity $\Delta\sigma \propto \tau^2\boldsymbol{E}\cdot\boldsymbol{B}$, which is nothing but the MCA. Experimentally, a very large MCA with $\gamma' \sim 4\times10^{-7}\ T^{-1}\,A^{-1}\,m^2$ has been observed in $ZrTe_5$ (13). This material is close to a topological phase transition and is described by the Dirac Hamiltonian, which is the origin of the giant MCA. Also, MCA can be enhanced in a nanowire with width ∼200 nm of topological insulator thin film $(Bi,Sb)_2Te_3$ with $\gamma \sim 10^5\ T^{-1}\,A^{-1}$ (14).

Instead of an external Zeeman magnetic field, MCA due to the magnetic moments or magnetic order has been explored. Yasuda et al. (15) observed MCA in the Cr-doped magnetic topological insulator heterostructure and attributed it to the asymmetric inelastic scattering by the magnons.

A similar mechanism has been proposed to explain the observed MCA in the ferromagnetic Rashba system (Ge,Mn)Te (16). MCA in the Rashba ferromagnet $PdCoO_2$ was also observed (17). Also, the elastic scattering by magnetic moments in noncentrosymmetric systems can induce MCA. MnSi, a ferromagnet with a chiral crystal structure, has a Dzyaloshinskii–Moriya interaction (DMI) showing a rich phase diagram in the plane of temperature T and magnetic field $\mathcal{B}$, including helical, conical, and skyrmion structures. MCA in this material was measured, which shows a nontrivial temperature and magnetic field dependence in the paramagnetic phase (18) and is attributed to chiral spin fluctuations. Theoretically, MCA by the spin cluster scattering was proposed (19), where the interference of the scattering waves from two spins produces an asymmetric transition probability $w_{\boldsymbol{k},\boldsymbol{k}'}$ from $\boldsymbol{k}$ to $\boldsymbol{k}'$. Namely,

$$w^{-}_{\boldsymbol{k}\sigma,\boldsymbol{k}'\sigma'} = \frac{1}{2}(w_{\boldsymbol{k}\sigma,\boldsymbol{k}'\sigma'} - w_{-\boldsymbol{k}\sigma,-\boldsymbol{k}'\sigma'}) \qquad 6.$$

becomes finite, which leads to MCA. More explicitly,

$$w^{-}_{\boldsymbol{k}\sigma,\boldsymbol{k}'\sigma'} \propto \sigma\delta_{\sigma,-\sigma'}(\boldsymbol{S}_i \times \boldsymbol{S}_j)_z, \qquad 7.$$

where the vector spin chirality $\boldsymbol{S}_i \times \boldsymbol{S}_j$ becomes finite due to the DMI representing the $\mathcal{P}$ breaking, and the electron spin σ is polarized by the external magnetic field $\mathcal{B}$. However, when the magnetic field $\mathcal{B}$ is too strong, the spins are aligned ferromagnetically, and hence $\boldsymbol{S}_i \times \boldsymbol{S}_j$ is reduced. $\boldsymbol{S}_i \times \boldsymbol{S}_j$ also decreases as the temperature is raised, and hence the MCA shows the peak structure at finite $\mathcal{B}$ and T in semiquantitative agreement with experiment (18). Note that the first-order Born approximation is enough for finite $w^{-}_{\boldsymbol{k}\sigma,\boldsymbol{k}'\sigma'}$ when both $\mathcal{P}$ and $\mathcal{T}$ are broken. Even a single magnetic impurity with spin–orbit interaction gives an asymmetric transition rate $w^{-}_{\boldsymbol{k}\sigma,\boldsymbol{k}'\sigma'}$ due to the toroidal moment (20). This is in sharp contrast to the $\mathcal{T}$-symmetric case, where $w^{-}_{\boldsymbol{k}\sigma,\boldsymbol{k}'\sigma'} = \frac{1}{2}(w_{\boldsymbol{k}\sigma,\boldsymbol{k}'\sigma'} - w_{-\boldsymbol{k}\sigma,-\boldsymbol{k}'\sigma'}) = \frac{1}{2}(w_{\boldsymbol{k}\sigma,\boldsymbol{k}'\sigma'} - w_{\boldsymbol{k}'\sigma',\boldsymbol{k}\sigma})$ can be finite only when the higher-order Born approximation is employed where the real transitions to the intermediate state occur (21). Also the "local" scalar spin chirality $\boldsymbol{S}_i \cdot (\boldsymbol{S}_j \times \boldsymbol{S}_k)$ associated with the noncoplanar magnetic ordering in bilayer triangular lattice was discussed as showing nonreciprocal resistivity even without the spin–orbit interaction, net scalar chirality, and net magnetization (22). Experimentally, the itinerant antiferromagnet $PdCrO_2$ showing 120-degree spin structure shows nonreciprocal resistivity (23).

Nonreciprocal transport in magnetic topological systems is also studied extensively, where the surface or edge states protected by the topology play a vital role. The nonlinear transport of the surface state of the magnetic topological insulator thin film was studied (24). This system shows the quantized anomalous Hall effect when the chemical potential is within the gap induced by the exchange coupling. Although this edge transport does not show any nonreciprocal effect, the scattering between the edge channels and the surface states becomes nonreciprocal. The heterostructure of helical edge channels of the two-dimensional quantum spin Hall insulator WTe_2 and the van der Waals antiferromagnet CrI_3 shows nonreciprocal transport (25).

From the fundamental viewpoint, several essential aspects of electronic states in solids, in addition to $\mathcal{P}$ and $\mathcal{T}$ symmetries, are relevant to nonreciprocity. The breaking of the unitary nature of time evolution and decoherence plays an important role for nonreciprocal transport as formulated in the nonequilibrium steady state of a many-body system coupled to the heat bath in terms of the Lindblad equation (26). The role of decoherence effects in nonreciprocal transport was discussed for mesoscopic electronic devices (27). Nonreciprocal interferometers have also been proposed (28).

It is also noted that the $\mathcal{P}$ and $\mathcal{T}$ symmetries are related to the geometric properties of the Bloch wave functions. Namely, when both $\mathcal{P}$ and $\mathcal{T}$ symmetries are intact, the Berry curvature

vanishes (1). In other words, the broken $\mathcal{P}$ and/or $\mathcal{T}$ is encoded by the Berry phase. A remarkable example of this fact is the modern theory of electric polarization; i.e., the electric polarization of the Bloch electrons is expressed by the Berry phase (29, 30). Therefore, the geometric nature of the Bloch electrons is relevant to the nonreciprocal responses. This is also the case of Landau–Zener tunneling where the Berry connections of conduction and valence bands give the nonreciprocal tunneling probabilities in noncentrosymmetric crystals without $\mathcal{T}$ breaking (31, 32). Another important nonreciprocal phenomenon related to the Berry phase is the nonlinear Hall effect (NLHE) (33), where the shifted Fermi surface induces the net anomalous velocity due to the Berry curvature dipole. Note that the NLHE does not require broken $\mathcal{T}$ symmetry. The combined effect of the dissipation and the geometric nature of the electronic states such as the quantum metric and Berry phase is relevant to the nonreciprocal transport (34). Non-Hermitian physics is also relevant (35). Nonreciprocal transport is closely related to the ratchet problem. A quantum mechanical particle motion in a periodic potential has been studied extensively, where the critical strength of the dissipation separating the classical localized ground state and the extended quantum ground state exists, i.e., the Schmid transition (36). When the periodic potential is asymmetric, the temperature dependence of the nonlinear mobility μ_2 defined by the velocity proportional to the applied electric field E strongly depends on the dissipation strength and goes to zero at zero temperature in the quantum regime, whereas μ_2/μ_1 (μ_1: linear mobility) remains finite at zero temperature in the classical regime (37, 38). This example suggests that the classical nature of the system is needed for nonreciprocal effects to a certain degree, and the duality between the particle nature and wave nature of quantum mechanics lies at the heart of the nonreciprocal responses.

From this viewpoint, electron correlations enhance the particle nature of the electrons leading to the tendency for localization, which induces nonreciprocity. Actually, the Coulomb interaction, even without $\mathcal{T}$ breaking, leads to the rectification effect. A classic example is the pn junction in which the width of the depletion layer depends on the direction of the applied voltage, where the Coulomb interaction is essential (39). Even without such an interface, the Coulomb interaction in multiband noncentrosymmetric crystals can give nonreciprocal transport, although the effect is usually very small (40).

3. NONRECIPROCAL EFFECTS IN SUPERCONDUCTORS

Superconductivity is one of the most "quantum" phenomena in solids showing totally dissipationless flow of electrons. Therefore, one might think that the nonreciprocal response is reduced in superconductors. However, nonreciprocity can be enhanced in superconductors (41). For example, the MCA is tremendously enhanced due to superconducting fluctuations as shown below. Furthermore, nonreciprocal charge transport unique to superconductors may occur, such as the superconducting diode effect (SDE), which is explained below.

3.1. Nonreciprocal Paraconductivity

In two-dimensional superconductors, there is a wide temperature region where the amplitude of the order parameter develops ($T < T_0$), and its phase becomes coherent ($T < T_{\mathrm{KT}}$). The latter is called the Kosterlitz–Thouless (KT) transition at which the binding of vortices and antivortices occurs. Near T_0, there occurs an additional conductivity σ_{para} due to the fluctuating order parameter, which is called paraconductivity. Because the fluctuation of the order parameter is regarded as classical at finite temperature even though its origin is quantum mechanical, this σ_{para} can be analyzed in terms of the time-dependent Ginzburg–Landau theory (42). One can expand the free energy in terms of the order parameter Ψ and also its momentum $\boldsymbol{p}$. Usually, we keep up to the second-order terms in $\boldsymbol{p}$, i.e., $\boldsymbol{p}^0$ and $\boldsymbol{p}^2$, because the odd-order terms are forbidden by

time-reversal symmetry $\mathcal{T}$. However, when both $\mathcal{T}$ and $\mathcal{P}$ are broken, odd-order terms are allowed, which leads to the nonreciprocity. The linear term in $\boldsymbol{p}$ shifts the momentum $\boldsymbol{p}_0$, which gives the minimum of the free energy, so $\boldsymbol{p} - \boldsymbol{p}_0$ plays the same role as $\boldsymbol{p}$. Therefore, the lowest-order terms that give nonreciprocal transport are third order. Ginzburg–Landau (GL) free energy has been derived explicitly for the transition metal dichalcogenide MoS_2 (43) considering that its band structure shows trigonal warping;

$$F = \int d^2r\Psi^*\left[a + \frac{p^2}{4m} + \frac{\Lambda\mathcal{B}}{\hbar^3}(p_x^3 - 3p_xp_y^3)\right]\Psi + \int d^2r\frac{b}{2}|\Psi|^4, \qquad 8.$$

where

$$\Lambda = \frac{93\zeta(5)}{28\zeta(3)}\frac{g\mu_B\Delta_{SO}\alpha}{\pi(k_BT_0)^2}, \qquad 9.$$

with α being the magnitude of the trigonal warping, Δ_{SO} the Ising spin splitting due to spin–orbit interaction, and Δ_z the Zeeman energy due to an external magnetic field. Employing the method developed by Schmidt (42), one can obtain the current due to the superconducting fluctuation up to the second order in the electric field $\boldsymbol{E}$ as

$$\boldsymbol{j} = \frac{e^2}{16\hbar\epsilon}\boldsymbol{E} - \frac{\pi e^3 m\Lambda\mathcal{B}}{64\hbar^3 k_BT_0\epsilon^2}\boldsymbol{F}(\boldsymbol{E}), \qquad 10.$$

with $\epsilon = (T - T_0)/T_0$ and $\boldsymbol{F}(\boldsymbol{E}) = (E_x^2 - E_y^2, 2E_xE_y)$. This corresponds to MCA, and its γ-value, γ_S, is substantially enhanced compared with that of the normal state γ_N, $\frac{\gamma_S}{\gamma_N} \sim \left(\frac{\varepsilon_F}{k_BT_0}\right)^3$, as expected from the change in the energy denominator from the Fermi energy ε_F to the superconducting gap $\Delta_{SC} \cong k_BT_0$. Experimentally, γ is negligible in the normal state, whereas at $T_0 \cong 9\,K$, $\gamma(T = 9\,K)$ reaches $\cong$1,000 $T^{-1}\,A^{-1}$, which is compared with the theoretical estimate $\gamma(T_0) \cong 400\ T^{-1}\,A^{-1}$ (43).

Below T_0, the amplitude of the order parameter develops, and the defects in its phase, i.e., vortices, determine the resistivity. Therefore, one can classify the mechanism of MCA in superconductors into paraconductivity and vortex dynamics, and the crossover between these two should occur as the temperature is decreased across T_0.

Theoretically, MCA in two-dimensional superconductors has been studied systematically for $T \gg T_0$ (normal state), $T > T_0$ (paraconductivity) and $T_{KT} < T < T_0$ (vortices) in the cases of (*a*) a Rashba superconductor, (*b*) a superconductor on the surface state of a topological insulator, and (*c*) transition metal dichalcogenides with Ising-type spin splitting, e.g., MoS_2 as shown in **Figure 1** (44). The MCA at $T < T_0$ depends on cases (*a*), (*b*), and (*c*), and also on the mechanism. In the cases of (*a*) and (*b*), MCA is induced by an in-plane magnetic field, whereas it is induced by an out-of-plane magnetic field in case (*c*). Accordingly, the KT transition survives in (*a*) and (*b*), whereas it becomes a crossover and the system remains resistive due to the vortices created by the external magnetic field in (*c*). Here, the ratchet mechanism for vortex motion assumes the classical diffusion motion of vortices under the asymmetric potential. In cases (*a*) and (*b*), the divergence of γ_S is predicted at both T_0 from below and T_{KT} from above, which originate from the modification of the superfluidity density ρ_S by the current I.

Experimentally, superconductivity in a Bi_2Te_3/FeTe interface has been studied (45). This two-dimensional superconductivity is classified as case (*b*), and shows a typical KT transition. MCA due to an in-plane magnetic field is observed, and γ shows critical behavior near T_{KT} as $\gamma \sim (T - T_{KT})^{-3/2}$ in agreement with the prediction (44). Gate-tuned $SrTiO_3$ is considered to be a Rashba superconductor [type (*a*)] and actually shows a very large MCA (46). It shows a crossover across T_0 from paraconductivity to the vortex region as T is lowered. γ is typically $\sim 10^4\ T^{-1}\,A^{-1}$ in the former region and $\sim 10^6\ T^{-1}\,A^{-1}$ in the latter. Recently, MCA in the interface of Bi_2Te_3/$PbTe_2$

		a Rashba SC ($B \perp \hat{z}$)	**b** TI surface + SC ($B \perp \hat{z}$)		**c** TMD ($B \parallel \hat{z}$)
Symmetry				**Hexagonal**	**Trigonal**
$T > T_0$	**Normal**	$V = a_1 I(1 + \gamma_N BI)$			
		$\gamma_N = 0 \quad (E_F > 0)$ $\gamma_N \sim \frac{\alpha}{e(m\alpha^2 E_{FR})^{3/2}} \quad (E_F < 0)$	$\gamma_N \sim \frac{\mathrm{sgn}\, E_F}{emv_F E_F^2}$	$\gamma_N \sim \frac{\lvert E_F \rvert \lambda}{ev_F^5}$	$\gamma_N \sim \frac{m\Delta_{SO}\lambda}{eE_F^3}$
	Paraconductivity	$V = a_1 I(1 + \gamma_S BI)$			
		Parity mixing ($E_F > 0$) $\gamma_S \sim \frac{r_{t,s} E_{F\alpha}}{eT_0^3 E_{FR} 1n(Ec/T_0)}$ ***q***-cubic term ($E_F < 0$) $\gamma_S \sim \frac{1}{em\alpha E_{FR} T_0}$	$\gamma_S \sim \frac{1}{emv_F E_F T_0}$	$\gamma_S \sim \frac{E_F^2 \lambda}{ev_F^5 T_0}$	$\gamma_S \sim \frac{m\Delta_{SO}\lambda}{eT_0^3}$
$T < T_0$		**KT transition**			**No KT transition**
		$T_{KT} < T < T_0$	$V = a_1 I(1 + \gamma_S BI)$ $\gamma_S \sim (T_0 - T) \quad (T \to T_0)$ $\gamma_S \sim (T - T_{KT})^{-3/2} \quad (T \to T_{KT})$		Viscous vortex flow $V = a'_1 BI(1 + \gamma_s BI)$ $\gamma_S \sim \frac{m\Delta_{SO}\lambda}{eT_0 E_F(T_0 - T)}$
		$T < T_{KT}$	$V = a_3 I^3 + a'_4 BI^4$		Ratchet mechanism $V = a'_1 BI(1 + \gamma'_s I)$

Figure 1

Nonreciprocal charge transport in two-dimensional noncentrosymmetric superconductors. There are three temperature regions (*a*, *b*, and *c*) classified by the mean-field superconducting transition temperature T_0 and KT transition temperature T_{KT}. Three cases are considered according to the symmetry. Figure adapted from Reference 44. Abbreviations: KT, Kosterlitz–Thouless; SC, superconductor; TI, topological insulator; TMD, transition metal dichalcogenide.

has been observed (47). The temperature and magnetic field dependence was analyzed in terms of thermally excited vortices and those created by the external magnetic field. In $PbTaSe_2$, the nonreciprocal transport is observed even at $\mathcal{B} = 0$, which is attributed to the asymmetric Hall effect of vortex–antivortex string pairs (48). MCA due to vortex motion was observed also in CsV_3Sb_5 (49). The centrosymmetric structure and symmetric electronic phases in this material indicate that the superconducting pairing breaks inversion symmetry. Application of MCA in the superconductor $NbSe_2$ to antennas from 5 to 900 MHz has been reported, which is also driven by vortex motion driven by AC electric field under an asymmetric pinning potential (50).

3.2. Bulk Diode

Although we have discussed nonreciprocal normal transport with a focus on the MCA, the nonreciprocal nature of superconducting response also attracts recent attention. This is realized when the critical current density along one direction $J_{c+} > 0$ is different from that along the opposite direction $J_{c-} < 0$ in terms of their magnitudes, namely, $J_{c+} \neq |J_{c-}|$. Below, we assume $J_{c+} > |J_{c-}|$ without any loss of generality. When we tune the magnitude of electric current density to lie between J_{c+} and $|J_{c-}|$, the electric current flows in one direction with zero resistance $R_+ = 0$ (supercurrent), whereas it flows in the opposite direction with finite resistance $R_- > 0$ (normal current), as illustrated in **Figure 2**. This unidirectional property of superconductivity

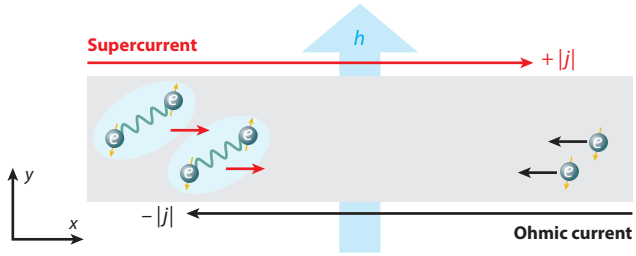

Figure 2

Schematic figure for the SDE. The system shows zero and finite resistance for the rightward and leftward currents, respectively. The directionality of the SDE is reversed when the magnetic field is reversed. Figure adapted from Reference 51. Abbreviation: SDE, superconducting diode effect.

has been recently called the SDE, and its discovery in the Nb/V/Ta superlattice has triggered vast research (52). Recent studies have observed the SDE in various superconductors, such as Rashba heterostructures (53, 54), transition metal dichalcogenides (55, 56), twisted multilayer graphene (57), conventional superconductors (58–63), and high-temperature cuprate superconductors (64). The SDE realizes perfect rectification in the sense that $R_-/R_+ = \infty$ and attracts attention as a candidate for an ideal diode.

Experimental platforms of the SDE are classified into bulk superconductors, as introduced above, and Josephson junctions (65). We focus on the bulk diode in this section. Various mechanisms of the bulk SDE have been studied in recent literature. Some of them essentially rely on the quality and geometry of samples, for example, the asymmetry of surfaces (59), asymmetric layer structures (61), and the asymmetric pinning centers (58). Such extrinsic mechanisms would be important when the critical current is determined by the vortex dynamics. A typical mechanism is the asymmetry of the vortex surface barrier and the corresponding critical current for vortex penetration (59, 66). Let us assume that the critical current density governed by one surface is j_c and that by the opposite surface is $j_c + \delta j_c > j_c$. Under the external and/or stray magnetic field, the Meissner current $\mp j_s$ asymmetrically modifies the critical current density as $j_{c\pm} \mp j_s = j_c$ for small j_s and $j_{c+} + j_s = j_c + \delta j_s$ and $j_{c-} + j_s = j_c$ for large j_s. This mechanism is ubiquitous in the sense that neither inversion symmetry breaking in the bulk, spin–orbit coupling, magnetization, nor finite-momentum Cooper pairs are needed. Indeed, the SDE by this mechanism has been observed in centrosymmetric superconductors (59, 60, 63) and in early studies (67–70). Conversely, it is hard to obtain information on the superconducting state via the SDE governed by this mechanism.

However, the intrinsic nature of superconductivity determines the depairing critical current, where the superconducting condensation energy and kinetic energy of the supercurrent are balanced. Therefore, the SDE due to the depairing critical current is called the intrinsic SDE. Experimentally, the depairing critical current can be realized in narrow samples compared with the Pearl length, $\Lambda = 2\lambda^2/d$ with penetration depth λ and sample thickness d (71–73). The intrinsic SDE has been intensively studied in recent theoretical works (51, 74–80) and revealed to be closely related to the quantum properties of superconductors. Therefore, we discuss the intrinsic SDE in the following part of this subsection.

The intrinsic SDE can be described by the GL theory, which is reliable near the transition temperature, $T \simeq T_c$, as usual. Here, we assume the superconducting order parameter with phase gradient along one direction, $\psi(x) = \psi e^{iqx}$, for simplicity. The GL free energy in the momentum space representation is given by

$$f(q, \psi) = \alpha(q)|\psi|^2 + \frac{\beta(q)}{2}|\psi|^4, \qquad 11.$$

with

$$\alpha(q) = \alpha_0 + \alpha_1 q + \alpha_2 q^2 + \alpha_3 q^3 + \alpha_4 q^4, \qquad \beta(q) = \beta_0 + \beta_1 q + \beta_2 q^2. \tag{12.}$$

The odd-order terms, α_1, α_3, and β_1, are allowed when $\mathcal{P}$ and $\mathcal{T}$ symmetries are broken. The present experiments on the bulk SDE have been carried out in this setup with broken $\mathcal{T}$ symmetry by an external magnetic field (52, 54, 55, 58–60, 62), ferromagnet/superconductor heterostructure (53, 56, 59, 60, 63), and valley polarization due to underlying electronic instability (57, 78). By contrast, the Josephson diode effect (JDE) has been reported sometimes in a $\mathcal{T}$ symmetric system (65) and is discussed in the next subsection. The GL free energy is minimized for each q as

$$f(q) = f\left(q, \sqrt{-\alpha(q)/\beta(q)}\right) = -\frac{\alpha(q)^2}{2\beta(q)}, \tag{13.}$$

when $\alpha(q) < 0$. The electric current $J(q)$ is calculated by $J(q) = -2\partial_q f(q)$, and the Cooper pairs' momentum in the equilibrium q_0 is obtained by solving the vanishing current condition, $J(q_0) = 0$. A finite-q superconducting state may be stable in equilibrium under broken $\mathcal{P}$ and $\mathcal{T}$ symmetries, owing to the first-order terms in q. This is called the helical superconducting state in noncentrosymmetric superconductors under magnetic fields (81, 82) and the anapole superconducting state in spontaneously symmetry-breaking superconductors (83). A typical example is the Rashba superconductor under an in-plane magnetic field, modeled by Equation 4, where the asymmetric band dispersion along the k_x axis makes the Cooper pairs' momentum, $\boldsymbol{q} = q_0\hat{x}$, finite.

The critical current in the $+x$ direction J_{c+} is determined by the maximum of $J(q)$, whereas that in the opposite $-x$ direction J_{c-} is by the minimum. To estimate J_{c+} and J_{c-}, it is convenient to expand $\alpha(q)$ and $\beta(q)$ for deviation from the equilibrium value at $T = T_c$ by defining $\delta q \equiv q - q_0$,

$$\alpha(q) = \alpha'_0 + \alpha'_2 \delta q^2 + \alpha'_3 \delta q^3, \qquad \beta(q) = \beta'_0 + \beta'_1 \delta q + \beta'_2 \delta q^2. \tag{14.}$$

The linear term in $\alpha(q)$ disappears in this expansion. The nonreciprocity of the critical current, namely, the SDE, is represented by $\Delta J_c = J_{c-} - |J_{c-}|$, and it is obtained as

$$\Delta J_c = \left(\frac{16}{27\beta'_0\alpha'_2}\alpha'_3 - \frac{8}{9\beta'^2_0}\beta'_1\right)\alpha'^2_0. \tag{15.}$$

As we see in Equation 15, the nonreciprocal critical current arises from α'_3 and β'_1. Because a finite value of q_0 combined with α_4 and β_2 makes α'_3 and β'_1 finite, the finite-momentum Cooper pairing in equilibrium is closely related to the SDE. However, the finite momentum q_0 is not necessary for the SDE, because it is also caused by the α_3 term, for example. Thus, details depend on the symmetry of systems. The generalized GL theory for the SDE (79) is applicable for all the noncentrosymmetric point group symmetry, and the SDE in the low magnetic field region is described by the "spin–orbit coupling" of Cooper pairs. Importantly, the SDE occurs in all the 21 noncentrosymmetric point groups, although the Cooper pairs' momentum can be zero in three of them, namely, nongyrotropic point groups, T_d, D_{3h}, and C_{3h}.

An index for the performance of the SDE is defined as $r \equiv (J_{c+} - |J_{c-}|)/(J_{c+} + |J_{c-}|)$ and is called the diode quality factor. The diode quality factor is tiny near the transition temperature for two reasons. First, as shown in Equation 15, the nonreciprocal critical current follows the scaling behavior $\Delta J_c \propto (T_c - T)^2$, which is higher order than the known scaling of the depairing critical current $J_{c\pm} \propto (T_c - T)^{3/2}$, leading to a vanishing diode quality factor at T_c, $r \propto (T_c - T)^{1/2}$. Second, in the isotropic Rashba superconductor, the SDE accidentally vanishes in the GL region (76). Therefore, anisotropic band dispersion, anisotropic Cooper pairing, and/or low temperature much below T_c is necessary for a sizable SDE.

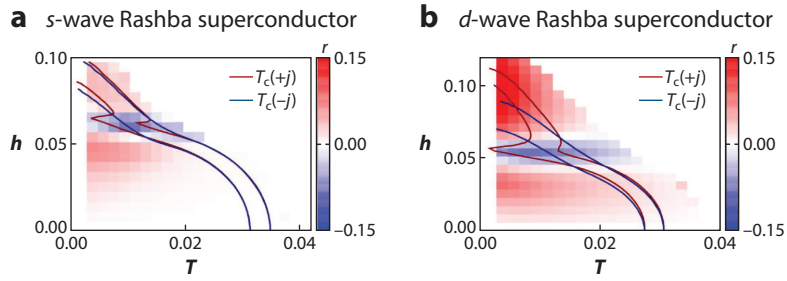

Figure 3

The diode quality factor r is plotted by color in the magnetic-field temperature phase diagram of (*a*) the *s*-wave superconducting state and (*b*) the *d*-wave superconducting state in the Rashba–Zeeman model. Nonreciprocal transition lines are also shown; red (blue) lines show T_c under the electric current $+j$ ($-j$) for several magnitudes j. Figure adapted with permission from Reference 79.

To discuss the intrinsic SDE in the whole temperature and magnetic-field region, we show the results of mean-field theory for the Rashba–Zeeman model, an analog of Equation 4 on the square lattice (51, 79). The diode quality factor is plotted as a function of the magnetic field and temperature in **Figure 3**. In the figure, we compare the *s*-wave Rashba superconductor and *d*-wave one. As expected from the above discussion, the diode quality factor is tiny in the *s*-wave superconductor at low magnetic fields near T_c, whereas it is enhanced in the *d*-wave superconductor due to the anisotropy of pair potential. In both cases, the diode quality factor is sizable, $r \simeq 0.15$, at low temperatures and high magnetic fields.

A more pronounced behavior is the sign reversal of the SDE in the moderate magnetic-field region. This sign reversal is caused by a crossover in the helical superconducting state (51), where the Cooper pairs' equilibrium momentum q_0 drastically increases. Thus, the observation of this sign reversal would be an experimental verification of the helical superconducting state, which has been long awaited after the theoretical prediction (81, 82). The sign reversal (polarity oscillation) in the SDE is indeed found in the Nb/V/Ta superlattice (54). However, the strength of the sign-reversal magnetic field is an order smaller than the theoretical prediction, and thus, further studies are desired. It is theoretically shown that the sign-reversal phenomenon is suppressed in moderately disordered superconductors (80), and therefore, a clean superconductor is desirable from this point of view. By contrast, the diode quality factor is enhanced by moderate disorders, and therefore, there is an optimum disorder to realize a significant SDE (80). The crossover phenomenon in the helical superconducting state also leads to an unusual phase diagram under the supercurrent, as shown in **Figure 3**. Accompanied by the sign reversal of the SDE, the critical temperature of superconductivity shows a significant nonreciprocity in the sense that T_c under the current $+J$ is different from that under $-J$. For a current direction, the superconductivity even shows a reentrant behavior similar to heavy fermion superconductors (84) (see **Figure 3**).

3.3. Josephson Diode

A Josephson junction with a weak link between the two superconductors offers a laboratory to study the interference of the phases of the order parameters. Namely, the phase difference ϕ between the two superconductors and the superconducting current I through the junction are related by the free energy $F(\phi)$ as $I = -\frac{2e}{\hbar}\frac{\partial F(\phi)}{\partial \phi}$ because of the canonical conjugate relation between the transferred charge Q and ϕ. Usually $F(\phi) \propto -\cos\phi$, and hence $I = I_c \sin\phi$ with I_c being the critical current above which the resistivity emerges. However, when the two sides of the Josephson junction are not symmetric, the critical current I_{c+} for positive direction and I_{c-} for negative direction

can be different; i.e., the Josephson diode effect (JDE) can occur. An early proposal for the JDE considered the junction between the electron-doped (n-type) and hole-doped (p-type) Mott insulators (85). The transition between the Mott insulating state and superconducting state can lead to the rectification effect under the bias voltage. Recently, the JDE has been revisited theoretically considering the asymmetry of the Coulomb energy associated with the charge transfer Q, i.e., the odd-order terms in Q (86). The charging energy corresponds to the kinetic energy of the dynamics of ϕ, but this can be neglected in the overdamped case. The "inertia" of ϕ leads to the hysteresis behavior of the current–voltage relation, and two critical currents I_{c1} and I_{c2} are defined. These critical currents depend on the direction with asymmetry of the Coulomb energy. Note that these two theoretical proposals do not require time-reversal symmetry breaking.

More recently, a general theory of the JDE has been proposed (87), where the JDE is classified into two types, i.e., (*a*) with broken $\mathcal{P}$ symmetry and (*b*) with broken $\mathcal{P}$ and $\mathcal{T}$ symmetries, corresponding to the classification of nonreciprocal responses in Reference 1. In type (*a*), $I_c(V) \neq I_c(-V)$ because the spin–orbit interaction at the tunneling barrier depends on the voltage V across the junction in addition to the original $\mathcal{P}$-symmetry breaking. In type (*b*), $I_{c+} \neq I_{c-}$ or $I_c(B) \neq I_c(-B)$ with B being the external magnetic field. An example is the magnetized electrons at the tunneling barrier, where the external magnetic field can change the magnitude of the magnetization and, hence, the Josephson coupling.

Another route to the JDE is the asymmetric free energy $F(\phi)$. For example, $F(\phi) = -J_1 \cos\phi + J_2 \sin 2\phi$ leads to $I = -\frac{2e}{\hbar}(J_1 \sin\phi + 2J_2 \cos 2\phi)$, and the minimum and maximum values of I are $I_{c+} \cong \frac{2e}{\hbar}(J_1 + 2J_2)$ and $-I_{c-} \cong -\frac{2e}{\hbar}(J_1 - 2J_2)$ up to the first order in J_2. Therefore, the J_2-term gives $I_{c+} \neq I_{c-}$. Note that the time-reversal operation $\mathcal{T}$ reverses the sign of ϕ because of the complex conjugation, and the J_2-term requires the $\mathcal{T}$-symmetry breaking. A possible model for this scenario is the JDE of *d*-wave superconductor/ferromagnetic insulator/*d*-wave superconductor on a three-dimensional topological insulator, where the direction of the *d*-wave lobes breaks $\mathcal{P}$ symmetry (88). The current–phase relation is influenced by the Majorana and Andreev bound states, and the quality factor $\eta = \frac{I_{c+} - I_{c-}}{I_{c+} + I_{c-}}$ reaches a value as large as $|\eta| \cong 0.4$ by tuning the angles of the *d*-wave lobes. A universal mechanism has been proposed in the diode effect in short Josephson junctions (89). The quality factor η defined above reaches up to 0.4, which arises from the Doppler shift of the Andreev bound state energies and the asymmetric current from the continuum. They also propose a scheme for finite-momentum pairing without spin–orbit interaction.

The JDE was first experimentally observed in Reference 65. The $I - V$ characteristics show hysteretic behavior, and the difference in the critical current ΔI_c between the opposite directions is an even function of the magnetic field B and finite even at $B = 0$. Wu et al. (65) argue that this effect can come from the nonreciprocal tunneling probability. Also the Josephson diode with memory based on an Nb superconductor was demonstrated at $B = 0$ (90). The diode efficiency is greater than 70%, which comes from the broken $\mathcal{P}$ and $\mathcal{T}$ symmetries by the self-field effect from nonuniform bias and a trapped Abrikosov vortex. Zero-field polarity-switchable Josephson diodes have also been realized where a proximity-magnetized Pt layer by ferrimagnetic insulating $Y_3Fe_5O_{12}$ induces the Rashba spin–orbit interaction (91). The quality factor reaches up to 35% at $T = 2$ K.

The search for the finite-momentum pairing is a long-standing keen issue, which can be relevant also to the Josephson junction. Related to this issue, a giant JDE has been realized in the finite-momentum pairing formed from a type-II Dirac semimetal, $NiTe_2$ (92). The nonreciprocity depends sensitively on the magnitude and direction of the magnetic field, which was interpreted as the Zeeman shift of spin-helical topological surface states and the consequent finite-momentum pairing state. It has been demonstrated that the highly transparent Josephson junctions fabricated on InAs quantum wells show the supercurrent rectification (93). The mechanism is that the

Josephson inductance L shows the MCA described as

$$L = L_0[1 + \gamma_L \boldsymbol{e}_z(\boldsymbol{B} \times \boldsymbol{I})], \tag{16.}$$

instead of the resistivity in Equation 3. Given the current–phase relation $I = I_{c0} f(\varphi)$, and the relation

$$L = V\left(\frac{\mathrm{d}I}{\mathrm{d}t}\right)^{-1} = \frac{\hbar}{2eI_{c0}}\left(\frac{\mathrm{d}f(\varphi)}{\mathrm{d}\varphi}\right)^{-1} = \frac{\hbar}{2e}\frac{\mathrm{d}\varphi(I)}{\mathrm{d}I}, \tag{17.}$$

Equation 16 leads to the MCA for supercurrent.

4. NONRECIPROCAL OPTICS

Onsager's reciprocal theorem, Equation 2, applied for optical response can describe nonreciprocal optical responses in which the direction of the propagation of light is specified by $\boldsymbol{q}$. For example, the natural circular dichroism in noncentrosymmetric materials is described by $\epsilon_{ij}(\boldsymbol{q}, \omega, \boldsymbol{B} = 0) \propto \varepsilon_{ijk} q_k$ with ε_{ijk} being the totally antisymmetric tensor. However, magneto-optical effects such as the Faraday effect and Kerr rotation are described by $\epsilon_{ij}(\boldsymbol{q} = 0, \omega, \boldsymbol{B}) \propto \varepsilon_{ijk} B_k$, and the magnetochiral effect by $\Delta\epsilon_{ii}(\boldsymbol{q}, \omega, \boldsymbol{B}) \propto \gamma_{ijk} q_j B_k$. All of these are linear responses, but here we discuss the nonlinear and nonreciprocal optical responses in noncentrosymmetric quantum materials (94–96). According to the classification in Reference 1, the nonreciprocal optical responses are categorized as (*a*) only $\mathcal{P}$ is broken, (*b*) both $\mathcal{P}$ and $\mathcal{T}$ are broken, and (*c*) both $\mathcal{P}$ and $\mathcal{T}$ are broken, while $\mathcal{PT}$ is not broken. We discuss case (*a*) in Section 4.1, cases (*b*) and (*c*) in Section 4.2, and the nonreciprocal optical responses in superconductors in Section 4.3.

4.1. Nonmagnetic Systems

In noncentrosymmetric materials, one expects a second-order nonlinear optical response of the current density J_a with respect to the electric field of light $\boldsymbol{E}$ as described by

$$J_a(\omega_1 + \omega_2) = \sigma^{(2)}_{abc}(\omega_1, \omega_2) E_b(\omega_1) E_c(\omega_2), \tag{18.}$$

where $\sigma^{(2)}_{abc}$ is the second-order nonlinear optical conductivity. The $\mathcal{P}$-symmetry breaking is often detected by second harmonic generation (SHG), where $\omega_1 = \omega_2 = \omega$. In contrast, the case of $\omega_1 = -\omega_2 = \omega$ leads to the DC response. The direct (DC) photocurrent I is usually driven by the applied DC electric field, which accelerates the photocarriers under light irradiation. Therefore, $I \propto |E(\omega)|^2 E_{\mathrm{DC}}$, a third-order nonlinear optical process. Recently, intensive studies, both experimentally and theoretically, have been done on the bulk photovoltaic effect, where the DC current second order in the electric field of light $E(\omega)$ without any DC electric field is induced (97–103).

In particular, the second-order nonlinear response for linearly polarized light is given by the formula (104):

$$\begin{aligned}\sigma^{(2)}_{abb}(\omega, -\omega) = -\frac{e^3}{\hbar^3\omega^2}\int \frac{\mathrm{d}\boldsymbol{k}^d}{(2\pi)^d}\Bigg[&\sum_{n,m}\frac{f_{nm}(\partial_{k_a} v_b)_{nm} v_{b,mn}}{\hbar\omega - \epsilon_{mn} + i\delta} \\ &+ \sum_{n,m,\ell\neq n}\frac{v_{a,n\ell} v_{b,\ell m} v_{b,mn}}{\epsilon_{n\ell}}\left(\frac{f_{nm}}{\hbar\omega - \epsilon_{mn} + i\delta} - \frac{f_{\ell m}}{\hbar\omega - \epsilon_{m\ell} - i\delta}\right)\Bigg] \\ &+ (\omega \leftrightarrow -\omega),\end{aligned} \tag{19.}$$

where $-e$ is the electron charge; the subscripts n, m, and ℓ specify the energy bands; and $f_{nm} = f(\epsilon_n) - f(\epsilon_m)$ with the Fermi distribution function and $\epsilon_{nm} = \epsilon_n - \epsilon_m$. Here, the energy

broadening δ is introduced phenomenologically. This expression is obtained in the velocity gauge, where $v_a = \partial_{k_a} H(k)$ along the a direction on the k-independent basis. The matrix element $v_{a,nm} = \langle u_n | v_a | u_m \rangle$ is related to that of the position operator r_a as

$$v_{a,nm} = i\epsilon_{nm} r_{a,nm}. \tag{20.}$$

In the length gauge, the matrix element $r_{a,nm}$ and its derivatives are used in the formulation (101), but the velocity gauge and length gauge are equivalent when all the bands are taken into account. Note that $\langle u_n | \partial_k v_a | u_m \rangle$ is different from $\partial_k \langle u_n | v_a | u_m \rangle$ because the Bloch wave functions depend on k.

In the presence of the $\mathcal{T}$ symmetry, Equation 19 is reduced to the following simple expression, which is called shift current:

$$J^{abb}_{shift} = -\frac{\pi e^3}{\hbar^3 \omega^2} |E_b(\omega)|^2 \sum_{nm} \int [\mathrm{d}\boldsymbol{k}] f_{nm} |v_{b,nm}|^2 R_{ab,mn} \delta(\hbar\omega - \epsilon_{mn}). \tag{21.}$$

The quantity $R_{ab,\,mn}$ is named shift vector and explicitly given by

$$R_{ab,mn} = \left[\frac{\partial}{\partial k_a} \mathrm{Im}(\log v_{b,nm}) + a_{a,m} - a_{a,n} \right]. \tag{22.}$$

The shift vector has a clear physical meaning, i.e., the shift of the center of the wave packet associated with the interband transition because the Berry connection $a_{a,n}$ represents the intracell coordinate. The first term in Equation 22 recovers the gauge invariance of the shift vector.

Shift current is closely related to the polarization current in ferroelectrics (29, 30, 105). In these geometric formulations, the electric polarization is given by the time integral of the polarization current and the integral of the Berry connection over the occupied states. The shift current is regarded as the change in the polarization due to the interband transitions, but the essential difference is that shift current can be direct current, whereas the polarization current is always AC. In order to support the steady DC shift current, relaxation is essential but not explicitly taken into account in the original perturbative treatment (100).

In order to study this issue, a two-band model has been treated in the Floquet formalism combined with Keldysh Green's function method (103). In this formulation, the optical transition is treated as the hybridization of the two bands 1 and 2 as

$$H_{\mathrm{F}} = \begin{pmatrix} \epsilon_1 + \omega & -iA^* v_{12} \\ iA v_{21} & \epsilon_2 \end{pmatrix}, \tag{23.}$$

where A and ω are the vector potential and frequency of light. Note here that the truncation of the Hilbert space into two dimensions is assumed at the level of k-independent basis such as the tight-binding model. This leads to a similar expression for the shift current (Equations 21 and 22) restricted to the two bands and with an additional factor

$$(\Gamma/2)/\sqrt{E^2 |v_{12}|^2/\omega^2 + \Gamma^2/4}, \tag{24.}$$

where E is the magnitude of the electric field $\boldsymbol{E}$ and Γ represents the relaxation that has no preference of direction. This factor represents the competition between the stimulated emission $\boldsymbol{E}^2 |v_{12}|^2/\omega^2$, which cancels the shift of the wave functions, and the neutral relaxation $\Gamma^2/4$. In the limit of weak electric field $\boldsymbol{E}$, this factor becomes 1, and apparently the relaxation plays no role but is essential for the steady-state DC current. This factor predicts the saturation behavior of the shift current as $\boldsymbol{E}$ is increased, i.e., crossover from $\propto \boldsymbol{E}^2$ to $\propto \boldsymbol{E}$. This crossover has been experimentally demonstrated in addition to the excellent agreement of the incident light energy dependence with the first-principles calculation in the polar semiconductor SbSI (106).

Considering that the shift current is similar to the polarization current, it does not require the photocarriers. Therefore, it can also be induced by the photoexcitation of the exciton without the DC external electric field. This possibility has been explored theoretically (107), and was later extended to the electromagnon in magnetic insulators (108). The idea is that both the polarization current and the shift current come from the virtual electron–hole excitation, and the mechanism to create this virtual transition in nonequilibrium steady state can induce the shift current. As for the exciton shift current, photocurrent has been observed at a peak energy of an exciton resonance in a semiconductor CdS (109). Furthermore, the phonon excitation in the ferroelectric material $BaTiO_3$ has been studied recently (110). The phonon excitation in the THz region induces virtual interband transitions via the electron–phonon interaction in this $\mathcal{P}$-broken system. It is found that the photocurrent does not depend on the external DC electric field, indicating that it is not from the photocarriers.

Another important issue is if the itinerant nature of the electronic states is essential for the shift current or not. Related to this issue, a recent experiment has revealed the robustness of the shift current against the disorder in the polar semiconductor SbSI (111). Even though the dark conductivity changes 7–8 orders of magnitude by varying the disorder strength, the photocurrent at zero bias remains almost unchanged (111). This strongly suggests that the shift current is supported also by localized states. The shift current in the disordered Rice–Mele model has been calculated numerically (112), and it is robust against localization as long as the nature of the conduction and valence bands is not mixed due to the disorder potential, which is in qualitative agreement with the experiment in SbSI (111). Materials showing a shift current are growing in number, including Weyl semimetals (113), transition metal dichalcogenides (114), and superconductors (115).

4.2. Magnetic Systems

Next, we discuss nonreciprocal optical responses in magnetic systems with broken $\mathcal{T}$ symmetry. We keep focusing on the second-order responses. Recent studies have shown some optical responses characteristic of magnetic systems, such as those categorized under the magnetophotogalvanic effect (MPGE) or spin-driven photocurrent. The photocurrent in magnetic systems is often accompanied by a finite photo-spin-current, enabling ultrafast spin manipulation. Therefore, the MPGE is also studied from the perspective of opto-spintronics.

Here, we review the classification of the photocurrent in $\mathcal{P}$-broken $\mathcal{T}$-symmetric systems and $\mathcal{P}$- and $\mathcal{T}$-broken $\mathcal{PT}$-symmetric systems. They correspond to cases (*a*) and (*c*) in the classification of nonreciprocal responses (Section 4.1). **Table 1** lists the photocurrent obtained by the dipole approximation and relaxation-time approximation. In case (*b*), $\mathcal{P}$-, $\mathcal{T}$-, and $\mathcal{PT}$-broken systems, all the responses in the table may occur. The Berry curvature dipole term and Drude

Table 1 Classification of photocurrent responses in metals, insulators, and superconductors with $\mathcal{T}$ symmetry or $\mathcal{PT}$ symmetry

System	$\mathcal{T}$-symmetric systems		$\mathcal{PT}$-symmetric systems	
Metal	Berry curvature dipole (116)	↻	Drude term (117)	↕
Metal and insulator	Electric injection current (101)	↻	Magnetic injection current (118)	↕
	Shift current (100, 101)	↕	Gyration current (119, 120)	↻
Superconductor	Berry curvature derivative (121)	↻	Nonreciprocal superfluid density (121)	↕
			Drude derivative (121)	↻

Abbreviations: ↻, circularly polarized-light-induced photocurrent; ↕, linearly polarized-light-induced photocurrent.

Table 2 Director X^μ and dipole-transition amplitude $T^{\nu\lambda}$ for the resonant photocurrent[a]

	X^μ	$T^{\nu\lambda}$
Electric injection current	Δ^μ	$\Omega^{\nu\lambda}$
Shift current	R^μ	$g^{\nu\lambda}$
Magnetic injection current	Δ^μ	$g^{\nu\lambda}$
Gyration current	$R^\mu_\pm$	$g^{\nu\lambda}$, $\Omega^{\nu\lambda}$

[a]The directors are group velocity difference Δ^μ, shift vector R^μ, and chiral shift vector $R^\mu_\pm$. The transition amplitude is characterized by the band-resolved quantum metric $g^{\nu\lambda}$ and Berry curvature $\Omega^{\nu\lambda}$. Table adapted from Reference 119.

term are counterparts of nonreciprocal transport discussed in Section 2, namely, the NLHE and MCA (122). Thus, they vanish in insulators but are allowed in metals. The injection current and shift current are resonant contributions and appear in insulators as well. In the systems without Kramers' degeneracy, these contributions lead to the photocurrent conductivity given by the overall formula

$$\sigma_{\mu\nu\lambda}(\Omega) \propto \int \mathrm{d}\boldsymbol{k} X^\mu T^{\nu\lambda} f_{mn} \delta(\hbar\Omega - \epsilon_{mn}), \tag{25.}$$

with director X^μ and transition amplitude $T^{\nu\lambda}$. The definitions of f_{mn} and ϵ_{mn} are given in Section 4.1. The list of X^μ and $T^{\nu\lambda}$ is shown in **Table 2**. The formula is modified in the presence of Kramers' degeneracy (119), which is the case for spinful $\mathcal{PT}$-symmetric systems.

Although the director of the shift current is the shift vector introduced in Section 4.1, it is the chiral shift vector (119, 120), a counterpart in the $\mathcal{PT}$-symmetric system, for the gyration (chiral shift) current. However, the velocity difference $\Delta^\mu_{mn}(\boldsymbol{k}) = v^\mu_{mm}(\boldsymbol{k}) - v^\mu_{nn}(\boldsymbol{k})$ is the director for the injection current. Thus, the shift current and injection current have essentially different characters. The shift current and gyration current are polarization currents related to the positional shift, whereas the injection current is related to the particle/hole motion due to the group velocity. As is known for the linear response, the transition amplitude also originates from the geometric properties of Bloch electrons, given by the band-resolved quantum metric $g^{\mu\nu}_{mn}$ and Berry curvature $\Omega^{\mu\nu}_{mn}$ defined as

$$g^{\mu\nu}_{mn} = \frac{1}{2}(a^\mu_{mn} a^\nu_{nm} + a^\mu_{mn} a^\nu_{nm}), \tag{26.}$$

$$\Omega^{\mu\nu}_{mn} = i(a^\mu_{mn} a^\nu_{nm} - a^\nu_{mn} a^\mu_{mn}). \tag{27.}$$

Therefore, it is naturally expected that the resonant photocurrent is enhanced in topological materials. This has been actually shown for tilted Dirac/Weyl fermions (119, 120). The photocurrent conductivity is divergent when the chemical potential lies close to the Dirac/Weyl points. The gyration current in the absence of Kramers' degeneracy can also be described by another geometric quantity, the symplectic Christoffel symbol (120).

Note that nonreciprocal optical responses may appear from mechanisms beyond the relaxation-time approximation. For example, second-order optical responses due to an extrinsic mechanism (21) and those carried by excitons (107) and electromagnons (108) have been studied.

An experimental search for the bulk MPGE has been carried out in recent studies, and it was observed in several setups, such as semiconductors (123, 124) and Dirac electrons (125) in the magnetic field, a ferromagnetic topological insulator (126), a magnetic multilayer (127), magnetic van der Waals heterostructures (128), and magnetic metamaterial (129). In Reference 129, control of the photogalvanic effect by polarization states of light and magnetization of electrons is demonstrated in a metamaterial, giving solid evidence for the bulk MPGE. Magnetically induced

response to the linearly polarized light is dominant, possibly corresponding to the magnetic injection current in **Table 1**. However, the long-wavelength approximation is not generally justified in metamaterials, leaving the microscopic origin unresolved.

4.3. Superconductors

Superconductors show anomalous electromagnetic properties that are absent in other materials. Indeed, the zero electric resistivity and the Meissner effect are fundamental properties defining superconductivity. Although these are linear responses, we may expect anomalous nonlinear responses as well.

In **Table 1**, we see the photocurrent unique to superconductors, such as that arising from the Berry curvature derivative (BCD) and nonreciprocal superfluid density (NRSF). These contributions arise from essential properties of superconductors; Bogoliubov quasiparticles are formed by the hybridization of electrons and holes. Because the electrons and holes have opposite electric charges, the vector potential derivative of the Bogoliubov–de Gennes (BdG) Hamiltonian is not equivalent to the momentum derivative, and thus, the (higher-order) current operators are

$$J^{\alpha_1\cdots\alpha_n} = (-1)^n \frac{\partial^n H_{\mathrm{BdG}}(\boldsymbol{k},\boldsymbol{A})}{\partial A^{\alpha_1}\cdots\partial A^{\alpha_n}}\Big|_{A=0} \neq \frac{\partial^n H_{\mathrm{BdG}}(\boldsymbol{k},\boldsymbol{0})}{\partial k^{\alpha_1}\cdots\partial k^{\alpha_n}}. \tag{28.}$$

The equality on the right-hand side is satisfied in the Bloch Hamiltonian in the normal state, and therefore, several terms vanish after the integration of momentum in the Brillouin zone (130). However, such a cancellation may not occur in superconductors, and as a consequence, anomalous terms appear in the electromagnetic response functions. Thus, we obtain anomalous nonreciprocal responses unique to superconductors (121). The zero resistivity and Meissner effect are also attributed to the same origin.

The anomalous nonreciprocal responses cause not only the photocurrent but also the SHG and difference-frequency generation. In $\mathcal{T}$-symmetric systems, anomalous nonreciprocal responses are given by the conductivity derivative (121),

$$\sigma^{\mathrm{sCD}}_{\alpha\beta\gamma}(\omega_1+\omega_2,\omega_1,\omega_2) = -\frac{i}{4}\left(\frac{1}{\omega_1}\partial_{\lambda_\beta}\sigma^{(\boldsymbol{\lambda})}_{\alpha\gamma} + \frac{1}{\omega_2}\partial_{\lambda_\gamma}\sigma^{(\boldsymbol{\lambda})}_{\alpha\beta}\right)\Big|_{\boldsymbol{\lambda}=0}, \tag{29.}$$

where $\sigma^{(\boldsymbol{\lambda})}_{\alpha\beta}$ is the normal linear conductivity, and $\boldsymbol{\lambda}$ is a virtual variable corresponding to the vector potential. For the photocurrent, $\omega_1 = -\omega_2 = \Omega$, in the low-frequency region, this term is reduced to the BCD,

$$\sigma^{\mathrm{BCD}}_{\alpha\beta\gamma}(\Omega) = \frac{i}{4\Omega}\epsilon_{\beta\gamma\delta}\partial_{\lambda_\alpha}\left(\sum_a \Omega^{\lambda_\delta}_a f_a\right)\Big|_{\boldsymbol{\lambda}=0}, \tag{30.}$$

with the total Berry curvature $\sum_a \Omega^{\lambda_\delta}_a f_a$ in the $\boldsymbol{\lambda}$ space. The BCD $\partial_{\lambda_\alpha}\left(\sum_a \Omega^{\lambda_\delta}_a f_a\right)$ is an axial rank-2 tensor and, thus, allowed in the gyrotropic point group. Note that the BCD is similar to the Berry curvature dipole (33) but different. Therefore, the BCD does not vanish in the gapped superconducting state.

When the $\mathcal{T}$ symmetry is broken, another response appears (121),

$$\sigma^{\mathrm{NRSF}}_{\alpha\beta\gamma}(\omega_1+\omega_2,\omega_1,\omega_2) = \frac{1}{2\omega_1\omega_2} f^{\alpha\beta\gamma}, \tag{31.}$$

which comes from the NRSF, $f^{\alpha\beta\gamma} = \partial_{\lambda_\alpha}\partial_{\lambda_\beta}\partial_{\lambda_\gamma}F_{\boldsymbol{\lambda}}$, obtained by the third-order derivative of free energy. Because the second-order derivative $\rho_{\mathrm{s}}^{\alpha\beta} = \partial_{\lambda_\alpha}\partial_{\lambda_\beta}F_{\boldsymbol{\lambda}}$ is the superfluid density, the NRSF can be regarded as the nonreciprocal correction to the superfluid density. As the superfluid density governs the Meissner effect, the NRSF makes the Meissner effect nonreciprocal in the sense that the Meissner response comprises a unidirectional component with respect to the magnetic

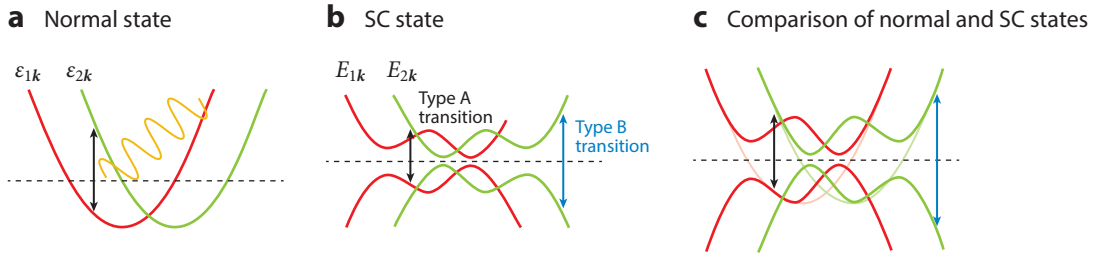

Figure 4

Illustration of optical transitions that may lead to the nonreciprocal optical responses. (*a*) Optical transition in the normal state. (*b*) Optical transitions in the superconducting state. Energy bands of Bogoliubov quasiparticles in single-band noncentrosymmetric superconductors are shown by E_{ik}. The type A and type B transitions contribute to the resonant nonreciprocal responses. The type A is $E_{ik} \leftrightarrow -E_{jk}$ $(i \neq j)$, which has a counterpart in the normal state. The type B is $E_{ik} \leftrightarrow -E_{ik}$, which is unique to superconductors. Thus, the superconducting nonreciprocal response needs the type B optical transition. (*c*) The comparison between the normal and superconducting states. Figure adapted from Reference 132. Abbreviation: SC, superconducting.

field (131). This is called the nonreciprocal Meissner effect. The NRSF $\hat{f}$ is a totally symmetric rank-3 tensor and odd parity for the symmetry operations $\mathcal{P}$ and $\mathcal{T}$. Therefore, the NRSF can be finite only when both $\mathcal{P}$ and $\mathcal{T}$ symmetries are broken. A detailed symmetry argument based on the point group is given in Reference 121.

Let us stress that the nonreciprocal optical responses due to the conductivity derivative and NRSF show low-frequency divergence, $\sigma^{\mathrm{sCD}}_{\alpha\beta\gamma} \propto 1/\omega$ and $\sigma^{\mathrm{NRSF}}_{\alpha\beta\gamma} \propto 1/\omega^2$. In contrast to the resonant contributions, which are also present in the normal state (Sections 4.1 and 4.2), topological structure in Bogoliubov quasiparticles is not needed for the divergent responses in the superconducting state. In this sense, the divergent nonreciprocal responses are ubiquitous in superconductors. Thus, giant photocurrent and SHG are expected to occur in the in-gap frequency region, typically from the sub-THz to THz range.

Microscopic conditions beyond symmetry arguments must be satisfied to obtain finite optical responses unique to superconductors. This can be intuitively understood by considering resonant contributions, for which interband optical transition is needed to occur. **Figure 4** illustrates the spectrum of Bogoliubov quasiparticles in noncentrosymmetric superconductors. The type B optical transition does not have a counterpart in the normal state, although the type A optical transition can be reduced to the normal optical transition by an adiabatic change from a superconducting state to a normal state. Therefore, some microscopic conditions have to be satisfied to allow the type B transition leading to the superconducting nonreciprocal responses. This expectation is verified by a microscopic calculation based on the BdG Hamiltonian (132), which has clarified microscopic conditions in noncentrosymmetric superconductors with $\mathcal{T}$ symmetry.[1] It is shown that the coexistence of interband Cooper pairs and intraband Cooper pairs is necessary. Furthermore, evaluating interband/intraband Cooper pairs in single-band noncentrosymmetric superconductors by superconducting fitness (134, 135), we see that spin-triplet Cooper pairs are necessary to cause nonreciprocal optical responses unique to superconductors (132). Because of this fact, nonreciprocal optics may be useful for probing spin-triplet Cooper pairs, which also play essential roles in superconducting spintronics (136) and topological superconductivity (137, 138), and so on.

Experimentally, a nonreciprocal optical phenomenon has been reported in a thin film of NbN (139). The SHG induced by supercurrent injection was observed and attributed to the

[1]See Reference 133 for the linear optical response in centrosymmetric superconductors.

ratchet motion of the vortices. By contrast, the nonreciprocal optical responses arising from the intrinsic properties of superconductors have not been identified to the best of our knowledge. Thus, experimental studies of superconducting nonreciprocal optics are a subject of current interest, and further research is awaited.

5. SUMMARY AND FUTURE PERSPECTIVES

We have discussed the nonreciprocal transport and optical phenomena in quantum materials. This field is newly and rapidly developing, expanding its horizon both theoretically and experimentally. Electronics is generally based on the nonlinear responses of electrons, e.g., diodes and transistors utilize the nonlinearity. Recently, most research focuses on bulk properties, although some are studying interfaces or junctions as discussed in Section 3.3. Momentum space geometry plays a major role in the nonreciprocal response of bulk states as repeatedly stated in this article. The generalization into spatially inhomogeneous structures, i.e., the coexistence of geometric structures in both momentum and real spaces, will be the next targets of research. In this case, the Berry connection in the phase space, i.e., six-dimensional r, k space, can play the central role (140). This includes artificial structures such as interfaces, surfaces, junctions, etc. Especially, the physical processes at the contacts with the electrodes are now well understood for the shift current, where the polarization current–like dc current in the bulk turns into the usual electron currents in the leads.

Another direction is the real time–dependent quantum phenomena. Most of this article focuses on steady-state properties independent of time, but the transient dynamics also contains a lot of information on the electronic states. Recent experimental advances in time-resolved spectroscopies such as angle-resolved photoemission spectroscopy (ARPES) are very useful in this respect, revealing new insight into the quantum dynamics.

Lastly, there still remain many issues unexplored in correlated electronic systems. This is a hard problem, even in the ground state or in thermal equilibrium, and hence the extension to the nonequilibrium seems even more difficult. However, a theoretical approach has been proposed, which is successful in some problems (141). It is likely that the time-dependent quantum dynamics of the correlated electrons can reveal important information that cannot be obtained by equilibrium properties, including new insight from linear response.

DISCLOSURE STATEMENT

The authors are not aware of any affiliations, memberships, funding, or financial holdings that might be perceived as affecting the objectivity of this review.

ACKNOWLEDGMENTS

The authors thank J. Ahn, A. Vishwanath, T. Morimoto, H. Ishizuka, Y. Okamura, N. Ogawa, Y. Kaneko, G.-Y. Guo, M. Nakamura, M. Kawasaki, Y. Tokura, Y. Takahashi, A. Daido, Y. Ikeda, H. Watanabe, H. Tanaka, F. Ando, Y. Miyasaka, R. Kawarazaki, H. Narita, T. Ono, and M. Matsubara for collaborations, and T. Arima and Y. Iwasa for useful discussion. N.N. was supported by JSPS KAKENHI grant 18H03676 and by JST CREST grant JPMJCR1874, Japan. Y.Y. was supported by JSPS KAKENHI (grants JP18H05227, JP18H01178, JP20H05159, JP21K18145, JP22H04933, and JP22H01181) and SPIRITS 2020 of Kyoto University.

LITERATURE CITED

1. Tokura Y, Nagaosa N. 2018. *Nat. Commun.* 9:3740
2. Orenstein J, Moore J, Morimoto T, Torchinsky D, Harter J, Hsieh D. 2021. *Annu. Rev. Condens. Matter Phys.* 12:247–72

3. Ideue T, Iwasa Y. 2021. *Annu. Rev. Condens. Matter Phys.* 12:201–23
4. Onsager L. 1931. *Phys. Rev.* 37(4):405–26
5. Kubo R. 1957. *J. Phys. Soc. Jpn.* 12(6):570–86
6. Rikken GLJA, Fölling J, Wyder P. 2001. *Phys. Rev. Lett.* 87(23):236602
7. Krstic V, Roth S, Burghard M, Kern K, Rikken GLJA. 2002. *J. Chem. Phys.* 117(24):11315–19
8. Rikken GLJA, Strohm C, Wyder P. 2002. *Phys. Rev. Lett.* 89(13):133005
9. Rikken GLJA, Wyder P. 2005. *Phys. Rev. Lett.* 94:016601
10. Ideue T, Hamamoto K, Koshikawa S, Ezawa M, Shimizu S, et al. 2017. *Nat. Phys.* 13(6):578–83
11. Li Y, Li Y, Li P, Fang B, Yang X, et al. 2021. *Nat. Commun.* 12:540
12. Morimoto T, Nagaosa N. 2016. *Phys. Rev. Lett.* 117(14):146603
13. Wang Y, Legg HF, Bömerich T, Park J, Biesenkamp S, et al. 2022. *Phys. Rev. Lett.* 128(17):176602
14. Legg HF, Roessler M, Muenning F, Fan D, Breunig O, et al. 2022. *Nat. Nanotechnol.* 17(7):696–700
15. Yasuda K, Tsukazaki A, Yoshimi R, Takahashi KS, Kawasaki M, Tokura Y. 2016. *Phys. Rev. Lett.* 117(12):127202
16. Yoshimi R, Kawamura M, Yasuda K, Tsukazaki A, Takahashi KS, et al. 2022. *Phys. Rev. B* 106(11):115202
17. Lee JH, Harada T, Trier F, Marcano L, Godel F, et al. 2021. *Nano Lett.* 21(20):8687–92
18. Yokouchi T, Kanazawa N, Kikkawa A, Morikawa D, Shibata K, et al. 2017. *Nat. Commun.* 8:866
19. Ishizuka H, Nagaosa N. 2020. *Nat. Commun.* 11:2986
20. Isobe H, Nagaosa N. 2022. *J. Phys. Soc. Jpn.* 91(11):115001
21. Isobe H, Xu SY, Fu L. 2020. *Sci. Adv.* 6(13):eaay2497
22. Hayami S, Yatsushiro M. 2022. *J. Phys. Soc. Jpn.* 91(9):063702
23. Akaike M, Nii Y, Masuda H, Onose Y. 2021. *Phys. Rev. B* 103(18):184428
24. Yasuda K, Morimoto T, Yoshimi R, Mogi M, Tsukazaki A, et al. 2020. *Nat. Nanotechnol.* 15(10):831–35
25. Zhao W, Fei Z, Song T, Choi HK, Palomaki T, et al. 2020. *Nat. Mater.* 19(5):503–7
26. Yamamoto K, Ashida Y, Kawakami N. 2020. *Phys. Rev. Res.* 2(4):043343
27. Bredol P, Boschker H, Braak D, Mannhart J. 2021. *Phys. Rev. B* 104(11):115413
28. Mannhart J. 2018. *J. Supercond. Novel Magn.* 31(6):1649–57
29. King-Smith RD, Vanderbilt D. 1993. *Phys. Rev. B* 47(3):1651–54
30. Resta R. 1994. *Rev. Mod. Phys.* 66(3):899–915
31. Kitamura S, Nagaosa N, Morimoto T. 2020. *Commun. Phys.* 3:63
32. Takayoshi S, Wu J, Oka T. 2021. *SciPost Phys.* 11:075
33. Du ZZ, Lu HZ, Xie XC. 2021. *Nat. Rev. Phys.* 3(11):744–52
34. Michishita Y, Nagaosa N. 2022. *Phys. Rev. B* 106(12):125114
35. Ashida Y, Gong Z, Ueda M. 2020. *Adv. Phys.* 69(3):249–435
36. Schmid A. 1983. *Phys. Rev. Lett.* 51(17):1506–9
37. Scheidl S, Vinokur VM. 2002. *Phys. Rev. B* 65(19):195305
38. Hamamoto K, Park T, Ishizuka H, Nagaosa N. 2019. *Phys. Rev. B* 99(6):064307
39. Ashcroft NW, Mermin ND. 1976. *Solid State Physics*. Fort Worth, TX: Harcourt Coll. 1st ed.
40. Morimoto T, Nagaosa N. 2018. *Sci. Rep.* 8:2973
41. Nadeem M, Fuhrer MS, Wang X. 2023. *Nat. Rev. Phys.* 5(9)558–77
42. Schmidt H. 1968. *Z. Phys. Hadrons Nuclei* 216(4):336–45
43. Wakatsuki R, Saito Y, Hoshino S, Itahashi YM, Ideue T, et al. 2017. *Sci. Adv.* 3(4):e1602390
44. Hoshino S, Wakatsuki R, Hamamoto K, Nagaosa N. 2018. *Phys. Rev. B* 98(5):054510
45. Yasuda K, Yasuda H, Liang T, Yoshimi R, Tsukazaki A, et al. 2019. *Nat. Commun.* 10:2734
46. Itahashi YM, Ideue T, Saito Y, Shimizu S, Ouchi T, et al. 2020. *Sci. Adv.* 6(13):eaay9120
47. Masuko M, Kawamura M, Yoshimi R, Hirayama M, Ikeda Y, et al. 2022. *NPJ Quantum Mater.* 7:104
48. Itahashi YM, Ideue T, Hoshino S, Goto C, Namiki H, et al. 2022. *Nat. Commun.* 13:1659
49. Wu Y, Wang Q, Zhou X, Wang J, Dong P, et al. 2022. *NPJ Quantum Mater.* 7:105
50. Zhang E, Xu X, Zou YC, Ai L, Dong X, et al. 2020. *Nat. Commun.* 11:5634
51. Daido A, Ikeda Y, Yanase Y. 2022. *Phys. Rev. Lett.* 128(3):037001
52. Ando F, Miyasaka Y, Li T, Ishizuka J, Arakawa T, et al. 2020. *Nature* 584(7821):373–76
53. Narita H, Ishizuka J, Kawarazaki R, Kan D, Shiota Y, et al. 2022. *Nat. Nanotechnol.* 17(8):823–28

54. Kawarazaki R, Narita H, Miyasaka Y, Ikeda Y, Hisatomi R, et al. 2022. *Appl. Phys. Express* 15(11):113001
55. Bauriedl L, Bäuml C, Fuchs L, Baumgartner C, Paulik N, et al. 2022. *Nat. Commun.* 13:4266
56. Yun J, Son S, Shin J, Park G, Zhang K, et al. 2023. *Phys. Rev. Res.* 5:L022064
57. Lin JX, Siriviboon P, Scammell HD, Liu S, Rhodes D, et al. 2022. *Nat. Phys.* 18(10):1221–27
58. Lyu YY, Jiang J, Wang YL, Xiao ZL, Dong S, et al. 2021. *Nat. Commun.* 12:2703
59. Hou Y, Nichele F, Chi H, Lodesani A, Wu Y, et al. 2023. *Phys. Rev. Lett.* 131:027001
60. Suri D, Kamra A, Meier TNG, Kronseder M, Belzig W, et al. 2022. *Appl. Phys. Lett.* 121(10):102601
61. Sundaresh A, Väyrynen JI, Lyanda-Geller Y, Rokhinson LP. 2023. *Nat. Commun.* 14:1628
62. Satchell N, Shepley PM, Rosamond MC, Burnell G. 2023. *J. Appl. Phys.* 133:203901
63. Gutfreund A, Matsuki H, Plastovets V, Noah A, Gorzawski L, et al. 2023. *Nat. Commun.* 14:1630
64. Mizuno A, Tsuchiya Y, Awaji S, Yoshida Y. 2022. *IEEE Trans. Appl. Supercond.* 32(6):6601005
65. Wu H, Wang Y, Xu Y, Sivakumar PK, Pasco C, et al. 2022. *Nature* 604(7907):653–56
66. Vodolazov DY, Peeters FM. 2005. *Phys. Rev. B* 72(17):172508
67. Touitou N, Bernstein P, Hamet JF, Simon C, Méchin L, et al. 2004. *Appl. Phys. Lett.* 85(10):1742–44
68. Vodolazov DY, Gribkov BA, Gusev SA, Klimov AY, Nozdrin YN, et al. 2005. *Phys. Rev. B* 72(6):064509
69. Morelle M, Moshchalkov VV. 2006. *Appl. Phys. Lett.* 88(17):172507
70. Papon A, Senapati K, Barber ZH. 2008. *Appl. Phys. Lett.* 93(17):172507
71. Sun Y, Ohnuma H, Ayukawa SY, Noji T, Koike Y, et al. 2020. *Phys. Rev. B* 101(13):134516
72. Nawaz S, Arpaia R, Lombardi F, Bauch T. 2013. *Phys. Rev. Lett.* 110(16):167004
73. Li J, Yuan J, Yuan YH, Ge JY, Li MY, et al. 2013. *Appl. Phys. Lett.* 103(6):062603
74. He JJ, Tanaka Y, Nagaosa N. 2022. *New J. Phys.* 24(5):053014
75. Yuan NFQ, Fu L. 2022. *PNAS* 119:e2119548119
76. Ilić S, Bergeret FS. 2022. *Phys. Rev. Lett.* 128(17):177001
77. Zinkl B, Hamamoto K, Sigrist M. 2022. *Phys. Rev. Res.* 4(3):033167
78. Scammell HD, Li JIA, Scheurer MS. 2022. *2D Mater.* 9(2):025027
79. Daido A, Yanase Y. 2022. *Phys. Rev. B* 106(20):205206
80. Ikeda Y, Daido A, Yanase Y. 2022. arXiv:2212.09211 [cond-mat.supr-con]
81. Bauer E, Sigrist M, eds. 2012. *Non-Centrosymmetric Superconductors: Introduction and Overview*. Berlin/Heidelberg: Springer Science & Business Media
82. Smidman M, Salamon MB, Yuan HQ, Agterberg DF. 2017. *Rep. Prog. Phys.* 80(3):036501
83. Kanasugi S, Yanase Y. 2022. *Commun. Phys.* 5:39
84. Aoki D, Brison JP, Flouquet J, Ishida K, Knebel G, et al. 2022. *J. Phys. Condens. Matter* 34(24):243002
85. Hu J, Wu C, Dai X. 2007. *Phys. Rev. Lett.* 99(6):067004
86. Misaki K, Nagaosa N. 2021. *Phys. Rev. B* 103(24):245302
87. Zhang Y, Gu Y, Li P, Hu J, Jiang K. 2022. *Phys. Rev. X* 12(4):041013
88. Tanaka Y, Lu B, Nagaosa N. 2022. *Phys. Rev. B* 106(21):214524
89. Davydova M, Prembabu S, Fu L. 2022. *Sci. Adv.* 8(23):eabo0309
90. Golod T, Krasnov VM. 2022. *Nat. Commun.* 13:3658
91. Jeon KR, Kim JK, Yoon J, Jeon JC, Han H, et al. 2022. *Nat. Mater.* 21(9):1008–13
92. Pal B, Chakraborty A, Sivakumar PK, Davydova M, Gopi AK, et al. 2022. *Nat. Phys.* 18(10):1228–33
93. Baumgartner C, Fuchs L, Costa A, Reinhardt S, Gronin S, et al. 2022. *Nat. Nanotechnol.* 17:39–44
94. Boyd RW. 2003. *Nonlinear Optics*. London: Academic
95. Bloembergen N. 1996. *Nonlinear Optics*. Singapore: World Sci.
96. Sturman BJ, Fridkin VM. 1992. *Photovoltaic and Photorefractive Effects in Noncentrosymmetric Materials*, Vol. 8. Philadelphia: CRC
97. Nie W, Tsai H, Asadpour R, Blancon JC, Neukirch AJ, et al. 2015. *Science* 347(6221):522–25
98. Shi D, Adinolfi V, Comin R, Yuan M, Alarousu E, et al. 2015. *Science* 347(6221):519–22
99. de Quilettes DW, Vorpahl SM, Stranks SD, Nagaoka H, Eperon GE, et al. 2015. *Science* 348(6235):683–86
100. von Baltz R, Kraut W. 1981. *Phys. Rev. B* 23(10):5590–96
101. Sipe JE, Shkrebtii AI. 2000. *Phys. Rev. B* 61(8):5337–52
102. Young SM, Rappe AM. 2012. *Phys. Rev. Lett.* 109(11):116601

103. Morimoto T, Nagaosa N. 2016. *Sci. Adv.* 2(5):e1501524
104. Parker DE, Morimoto T, Orenstein J, Moore JE. 2019. *Phys. Rev. B* 99(4):045121
105. Vanderbilt D, King-Smith RD. 1993. *Phys. Rev. B* 48(7):4442–55
106. Sotome M, Nakamura M, Fujioka J, Ogino M, Kaneko Y, et al. 2019. *PNAS* 116(6):1929–33
107. Morimoto T, Nagaosa N. 2016. *Phys. Rev. B* 94(3):035117
108. Morimoto T, Nagaosa N. 2019. *Phys. Rev. B* 100(23):235138
109. Sotome M, Nakamura M, Morimoto T, Zhang Y, Guo GY, et al. 2021. *Phys. Rev. B* 103(24):L241111
110. Okamura Y, Morimoto T, Ogawa N, Kaneko Y, Guo GY, et al. 2022. *PNAS* 119(14):e2122313119
111. Hatada H, Nakamura M, Sotome M, Kaneko Y, Ogawa N, et al. 2020. *PNAS* 117:20411
112. Ishizuka H, Nagaosa N. 2021. *PNAS* 118(10):e2023642118
113. Osterhoudt GB, Diebel LK, Gray MJ, Yang X, Stanco J, et al. 2019. *Nat. Mater.* 18(5):471–75
114. Akamatsu T, Ideue T, Zhou L, Dong Y, Kitamura S, et al. 2021. *Science* 372(6537):68–72
115. Xu T, Morimoto T, Moore JE. 2019. *Phys. Rev. B* 100(22):220501
116. Moore JE, Orenstein J. 2010. *Phys. Rev. Lett.* 105(2):026805
117. Holder T, Kaplan D, Yan B. 2020. *Phys. Rev. Res.* 2(3):033100
118. Zhang Y, Holder T, Ishizuka H, de Juan F, Nagaosa N, et al. 2019. *Nat. Commun.* 10:3783
119. Watanabe H, Yanase Y. 2021. *Phys. Rev. X* 11:011001
120. Ahn J, Guo GY, Nagaosa N. 2020. *Phys. Rev. X* 10(4):041041
121. Watanabe H, Daido A, Yanase Y. 2022. *Phys. Rev. B* 105(2):024308
122. Watanabe H, Yanase Y. 2020. *Phys. Rev. Res.* 2(4):043081
123. Ogawa N, Bahramy MS, Murakawa H, Kaneko Y, Tokura Y. 2013. *Phys. Rev. B* 88(3):035130
124. Burger AM, Agarwal R, Aprelev A, Schruba E, Gutierrez-Perez A, et al. 2019. *Sci. Adv.* 5:eaau5588
125. Olbrich P, Zoth C, Vierling P, Dantscher KM, Budkin GV, et al. 2013. *Phys. Rev. B* 87(23):235439
126. Ogawa N, Yoshimi R, Yasuda K, Tsukazaki A, Kawasaki M, Tokura Y. 2016. *Nat. Commun.* 7:12246
127. Li G, Mikhaylovskiy RV, Grishunin KA, Costa JD, Rasing T, Kimel AV. 2018. *J. Phys. D Appl. Phys.* 51(13):134001
128. Song T, Anderson E, Tu MWY, Seyler K, Taniguchi T, et al. 2021. *Sci. Adv.* 7(36):eabg8094
129. Matsubara M, Kobayashi T, Watanabe H, Yanase Y, Iwata S, Kato T. 2022. *Nat. Commun.* 13:6708
130. Michishita Y, Peters R. 2021. *Phys. Rev. B* 103(19):195133
131. Watanabe H, Daido A, Yanase Y. 2022. *Phys. Rev. B* 105(10):L100504
132. Tanaka H, Watanabe H, Yanase Y. 2023. *Phys. Rev. B* 107(2):024513
133. Ahn J, Nagaosa N. 2021. *Nat. Commun.* 12:1617
134. Ramires A, Sigrist M. 2016. *Phys. Rev. B* 94(10):104501
135. Ramires A, Agterberg DF, Sigrist M. 2018. *Phys. Rev. B* 98(2):024501
136. Linder J, Robinson JWA. 2015. *Nat. Phys.* 11(4):307–15
137. Tanaka Y, Sato M, Nagaosa N. 2012. *J. Phys. Soc. Jpn.* 81:011013
138. Sato M, Fujimoto S. 2016. *J. Phys. Soc. Jpn.* 85(7):072001
139. Nakamura S, Katsumi K, Terai H, Shimano R. 2020. *Phys. Rev. Lett.* 125(9):097004
140. Xiao D, Chang MC, Niu Q. 2010. *Rev. Mod. Phys.* 82(3):1959–2007
141. Aoki H, Tsuji N, Eckstein M, Kollar M, Oka T, Werner P. 2014. *Rev. Mod. Phys.* 86(2):779–837